Title

Degradation Mechanisms of Fluorinated Disordered Rocksalt Cathodes: Effects of Electrolyte Chemistry and Discharge Voltage

Journal

ACS Applied Materials & Interfaces, 18(34)

ISSN

1944-8244

Authors

Ahmed, Ridwan A

Lee, Gi-Hyeok

Hershkovitz, Eitan

et al.

Publication Date

2026-09-02

DOI

10.1021/acsami.6c09846

Degradation Mechanisms of Fluorinated Disordered Rocksalt Cathodes: Effects of Electrolyte Chemistry and Discharge Voltage

Ridwan A. Ahmed[1,#], Gi-Hyeok Lee[2,#], Eitan Hershkovitz[3], Tianyu Li[4], Yanbao Fu[5], Isiksu Buyuker[6], Mateusz Zuba[6], Ozgenur Kahvecioglu[6], Vincent S. Battaglia[5], Raphaële J. Clément[4,7]*, Wanli Yang[2,]*, Chongmin Wang[3,]*, and Wu Xu[1,]*

[1] Energy and Environment Directorate, Pacific Northwest National Laboratory, Richland, WA 99354, USA

[2] Advanced Light Source, Lawrence Berkeley National Laboratory, Berkeley, CA 94720, USA

[3] Environmental Molecular Sciences Laboratory, Pacific Northwest National Laboratory Richland, WA 99354, USA

[4] Materials Department and Materials Research Laboratory, University of California Santa Barbara, CA 93106, USA

[5] Energy Storage and Distributed Resources Division, Lawrence Berkeley National Laboratory, Berkeley, CA 94720, USA

[6] Applied Materials Division, Argonne National Laboratory, Lemont, IL 60439, USA

[7] Max Planck Institute for Solid State Research, Stuttgart 70569, Germany

[#] These authors contributed equally to this work.

* Corresponding authors. Emails: rclement@ucsb.edu (R. J. Clément), wlyang@lbl.gov (W. Yang), chongmin.wang@pnnl.gov (C. Wang), wu.xu@pnnl.gov (W. Xu)

KEYWORDS: disordered rock-salt cathode, electrolyte, discharge cutoff voltage, structural integrity, interphase, high voltage

ABSTRACT

Cation-disordered rock-salt (DRX) oxides have emerged as a promising class of high energy density cathodes for next-generation lithium-ion batteries. Fluorination has been widely employed to tune the redox chemistry and structural stability of these materials, leading to enhanced electrochemical performance. However, the degradation mechanisms of fluorinated DRX (F-DRX) cathodes during electrochemical cycling remain poorly understood. Here, we investigate the degradation behavior of an F-DRX cathode cycled in a conventional carbonate-based electrolyte and a localized high-concentration electrolyte (LHCE). By correlating electrochemical performance with interfacial and bulk structural evolution, we elucidate the role of electrolyte chemistry and deep discharge voltage in governing structural transformation and degradation. The results reveal more pronounced surface and bulk structural changes in the conventional $LiPF_6$-carbonate electrolyte relative to LiFSI-LHCE, indicating accelerated degradation in the former. Lowering the discharge cutoff voltage from 2.0 V to 1.5 V further promotes interfacial degradation in both electrolyte systems. This work demonstrates that the LHCE offers superior compatibility with F-DRX cathodes, enabling stable cycling by mitigating surface and bulk structural degradation. These insights clarify the interplay between electrolyte chemistry and voltage window in F-DRX degradation and highlight the critical importance of advanced electrolyte designs for unlocking the full potential of DRX cathodes.

1. Introduction

The growing deployment of lithium (Li)-ion batteries (LIBs) across transportation, grid-scale storage, and aerospace applications has intensified the demand for cathode materials that simultaneously offer high capacity, high energy density, and reduced cost. Conventional layered transition metal (TM) oxide cathodes, while commercially mature, are intrinsically constrained by a strong reliance on scarce and expensive TMs such as cobalt and nickel. This motivates the exploration of alternative cathode chemistries capable of delivering higher energy density with improved material sustainability.[1-3]

Cation-disordered rock-salt (DRX) oxides have emerged as a promising class of next-generation cathode materials due to their ability to deliver high reversible capacities at elevated voltages.[4-6] Unlike layered cathodes, the disordered rock-salt framework tolerates a broad range of TMs enabling the incorporation of earth-abundant and low-cost elements.[6-9] This offers a viable pathway toward lowering cathode cost while achieving high energy density, making DRX materials attractive for large-scale energy storage applications. Despite these advantages, DRX cathodes suffer from intrinsically poor electrochemical stability. The participation of oxygen (O) redox, while essential for accessing high capacity, often induces irreversible O loss, and TM migration, ultimately compromising both structural integrity and electrochemical reversibility.[10-12] These bulk and interfacial degradation processes are frequently accompanied by aggressive parasitic reactions between the highly reactive DRX surface and conventional carbonate-based electrolytes, leading to unstable cathode-electrolyte interphases (CEIs) and accelerated performance decay.[10, 13, 14] Such degradation mechanisms are commonly manifested as surface disorder, and bulk structural changes, which are readily captured by scanning transmission electron microscopy (STEM) and soft X-ray absorption spectroscopy (sXAS) measurements.

Partial substitution of O with fluorine (F) has been shown to modify anionic redox behavior, strengthen metal cation-anion bonding, and suppress irreversible O loss, thereby improving structural robustness and cycling stability.[15-17] Fluorinated DRX (F-DRX) materials have demonstrated improved electrochemical performance and enhanced energy density relative to their non-fluorinated counterparts.[18-21] However, there is growing evidence that fluorine incorporation into DRX is significantly lower than the intended level, particularly for Mn-rich DRX compositions.[19, 22] Meanwhile, F-DRX cathodes still undergo substantial degradation during cycling, particularly in conventional carbonate electrolytes, indicating that fluorination alone does not fully mitigate structural instability or electrolyte-induced interfacial reactions.[23-25] Hence, a systematic investigation of the degradation mechanisms in F-DRX cathodes, and their dependence on electrolyte chemistry and operating voltage window, is timely.

In this work, we provide a systematic mechanistic investigation of F-DRX degradation in Li‖F-DRX cells cycled with a conventional electrolyte (1 M $LiPF_6$ in ethylene carbonate (EC) and dimethyl carbonate (DMC) at 1:2 by wt.), as well as with a LiFSI-2DMC-0.2EC-3TTE (1,1,2,2-

tetrafluoroethyl-2,2,3,3-tetrafluoropropyl ether) by mol.) electrolyte, in the voltage range of 1.5 – 4.8 V and 2.0 – 4.8 V. The LiFSI-2DMC-0.2EC-3TTE electrolyte contains a diluent TTE that dilutes the high concentration electrolyte to form what is generally referred to as the LHCE [26,27]. The resulting solvation structure is typically dominated by the presence of contact ion pairs (CIPs) and Aggregates (AGGs) which differ from the conventional electrolyte dominated by solvent-separated ion pairs (SSIPs) as discussed in our prior works [26, 28, 29].

By correlating electrochemical performance with surface and bulk structural characterizations, we directly link electrolyte chemistry to surface and bulk structural disorder in F-DRX cathodes. Furthermore, by comparing cycling to the discharge cutoff of 2.0 V and 1.5 V, we elucidate the effects of deep discharge on the degradation mechanisms of F-DRX cathodes in both electrolyte systems.

The results demonstrate that the performance of the F-DRX cathode strongly depends on electrolyte chemistry. The conventional electrolyte facilitates irreversible redox processes and coupled surface and bulk structural changes. These processes cause rapid impedance growth and accelerated capacity decay in Li||F-DRX cells. In contrast, the LHCE effectively maintains redox reversibility and mitigates both interfacial and bulk structural degradation, thereby enabling significantly enhanced electrochemical stability. Deep discharge to 1.5 V further intensifies irreversible redox activity, particularly in the conventional electrolyte when compared with a 2.0 V cutoff, which in turn exacerbates resistance buildup and capacity loss. However, the extent of this voltage-induced degradation remains secondary to the predominant influence of electrolyte composition. This study establishes a direct structure-chemistry-electrochemistry relationship for F-DRX cathodes, identifies electrolyte-dependent degradation mechanisms, and provides concrete design principles for advanced electrolytes capable of stabilizing F-DRX cathodes for practical LIB applications.

2. Materials and Methods

2.1 F-DRX Synthesis

Precursors of Mn_2O_3 at 60 mol%, TiO_2 at 20 mol%, Li_2CO_3 at 110 mol%, and LiF at 20 mol% (where total Li content from Li_2CO_3 and LiF was 130 mol%) adding up to ~200 g were ball-milled together with Y-stabilized ZrO_2 in 500 mL jars at 100 RPM using Retsch Planetary Ball Mill PM 400. The milled precursors were calcined at 900 °C for 10 h using a ramp rate of 5 ºC min^{-1} under an argon (Ar) atmosphere. Calcination was done as loose powder at 30-g scale. The calcined F-DRX material was subsequently ball-milled at 400 RPM in an organic solvent for 4 h without any carbon. The ball-milled material was recovered, dried, and sieved using 45-micron mesh. All processes were conducted at the Materials Engineering Facility (MERF) at Argonne National Laboratory (ANL). The composition of the final powder product was characterized to be $Li_{1.18}Mn_{0.63}Ti_{0.19}O_{1.90}F_{0.10}$ as elucidated in section 3.1.

2.2 Electrolyte and Electrode Preparation

The conventional electrolyte (1 M $LiPF_6$ in EC-DMC, 1:2 by wt.) and the LHCE (LiFSI-2DMC-0.2EC-3TTE, by mol.) were prepared by dissolving $LiPF_6$ in an EC-DMC mixture or LiFSI in a DMC-EC-TTE mixture, respectively based on the designed weight or molar ratio. All electrolyte preparation was carried out in an Ar-filled MBraun glovebox (O_2 < 1 ppm and H_2 < 1 ppm). The F-DRX electrode laminates were fabricated in the Lawrence Berkeley National Laboratory (LBNL) facility with 75 wt.% F-DRX powder as active material, 10 wt.% Denka black (DB), 5 wt.% carbon nanotube (CNT) and 10 wt.% PEDOT. The resulting laminates had an areal mass loading of 4.8 mg cm^{-2} and were punched into 12.7 mm. The electrodes were dried under vacuum at a temperature of 130 ºC for at least 12 h before use. Li metal chips with a thickness of 250 µm and a diameter of 15.5 mm were purchased from MTI Corporation USA and used as received.

2.3 Electrochemical Tests

Li||F-DRX coin cells were assembled using an F-DRX cathode disk (12.7 mm diameter), a polyethylene separator, a 250 µm thick Li metal anode, and 75 µL electrolyte. An Al-clad positive case was employed, with an additional Al foil (19.0 mm diameter) inserted between the positive case and the F-DRX cathode disk to prevent anodic corrosion of the stainless-steel positive case at high voltages. For the electrochemical cycling stability tests, the cells were first subjected to four formation cycles at a current density of 10 mA g^{-1}, followed by long term cycling at 20 mA g^{-1}.

For the DCIR measurement, Li‖F-DRX cells were assembled following the same protocol as used for the cycling stability tests. After four formation cycles, the DCIR protocol was implemented on the 5th cycle. Specifically, the cells were charged at a slow rate of 4 mA g^{-1} to 50% state of charge (SOC), followed by a 100 mA g^{-1} current pulse applied for 30 seconds. The charge rate was then returned to 4 mA g^{-1} for the rest of the cycle. Subsequently, the cells were cycled under standard conditions at 20 mA g^{-1} until the 30th cycle, at which point the same DCIR pulse sequence was repeated. This procedure was performed again on the 120th cycle, enabling the determination of DCIR at the 5th, 30th and 120th cycles to monitor the evolution of internal resistance during long-term cycling.

2.4 Scanning Transmission Electron Microscopy (STEM) and Energy Dispersive X-Ray Spectroscopy (EDS)

For STEM imaging, the pristine and cycled particles were dispersed onto TEM lacey carbon grids in an Ar-filled glovebox. HAADF-STEM imaging was performed using an aberration-corrected Spectra (Thermo Fisher) microscope. The accelerating voltage of the microscope was 300 keV, and the semi-convergence angle was 30 mrad. EDS data was collected using a Thermo Fisher Ultra-X detector with a 4.04 srad solid angle.

2.5 Soft X-ray Absorption Spectroscopy (sXAS)

C and O K-edges, and Mn L-edge sXAS spectra were collected at beamline 8.0.1 in Advanced Light Source, LBNL. The samples charged at various states and cycles were transferred to the glovebox for sampling and pasted on the Cu tape for the measurement. An airtight transfer kit was used to transfer the sample from the glovebox to the measurement chamber. The incident beam size was approximately 100 micrometers (horizontal) by 50 micrometers (vertical), and the measurements were performed at a 45-degree sample tilt angle. This configuration yielded a large beam footprint that inherently probed an ensemble average of multiple cathode particles.

For the C and O K-edge sXAS spectra collection, total fluorescence yield (TFY; detecting less than 200 nm from the surface) and total electron yield (TEY; detecting less than 10 nm from the surface) modes were used, and the reported spectra represent the average of 3 repeated scans at a single location. For the F K-edge spectra, 5 repeated scans were averaged to enhance the signal-to-

noise ratio. For the Mn L-edge, TEY mode and map of resonant inelastic X-ray scattering-inverse partial fluorescence yield (mRIXS-iPFY) mode were used, where a single scan was recorded with a long dwelling time of 80 seconds per energy point to ensure sufficient data quality.

Map of resonant inelastic X-ray scattering-inverse partial fluorescence yield (mRIXS-iPFY) Mn-L3 mRIXS-iPFY was extracted through the formula iPFY = a / PFY_O, where a is a normalization coefficient, and PFY_O is extracted by integrating the fluorescence intensity within the O-K emission energy range (490 to 530 eV) on the Mn-L_3 mRIXS. Mn-L_3 mRIXS-iPFY was used in this work instead of TFY to avoid the distortion observed in the conventional TFY caused by emission signals from oxygen.[30]

2.6 Solid-State Nuclear Magnetic Resonance (NMR) Spectroscopy

^{7}Li and ^{19}F solid-state NMR spectra of the pristine and ^{7}Li solid-state NMR spectra cycled LMTF cathodes cycled with E-baseline and LHCE were acquired using a wide bore Bruker BioSpin spectrometer charged to 2.35 T (100 MHz for ^{1}H) and equipped with a DMX 500 MHz console and a custom-made 1.3 mm, single channel broadband magic angle spinning (MAS) probe tuned to ^{7}Li (38.9 MHz) or ^{19}F (94.1 MHz). NMR spectra were obtained at 60 kHz magic angle spinning (MAS) using a rotor synchronized spin-echo sequence ($90° - \tau_r - 180° - \tau_r$), with 90° radio frequency (RF) pulses of 0.45 μs for ^{7}Li and 0.3 μs for ^{19}F. ^{7}Li chemical shifts were externally referenced against a 1 M aqueous LiCl solution (δ_{iso} = 0 ppm). ^{19}F chemical shifts were referenced against a 1 M aqueous NaF solution (δ_{iso} = −118.14 ppm). For ^{7}Li, a recycle delay of 20 s was used throughout, sufficiently long for all spins to re-equilibrate between scans, providing quantitative spectra. For ^{19}F, both a short recycle delay of 20 ms and a long recycle delay of 10 s were used. A 20 ms recycle delay was applied to maximize the paramagnetic signal from F in the F-DRX structure. The long recycle delay was used to enable quantitative analysis of the F content in both the DRX phase and in the LiF impurity. All battery disassembly and sample loading steps were conducted in Ar-filled glovebox, and rotors were spun using dry nitrogen. NMR spectra were processed using the Bruker TopSpin 3.6.0 software.

3. Results and Discussion

3.1 Characterization of the Nano-sized F-DRX Material

Nano-sized F-DRX was synthesized via a conventional solid-state reaction followed by high-energy ball milling without any carbon (C). High-temperature calcinations are needed to fully disorder solid-state precursors, but will also lead to Li & F-loss during synthesis due to increased volatility. At the same time, fluorine solubility in DRX is limited and compositionally dependent often leading to batch-to-batch variability. Therefore, detailed synthesis procedures and materials processing conditions are provided in the materials and methods section. Additionally, the structure, morphology, and composition of the as-synthesized F-DRX material, with a targeted stoichiometry of $Li_{1.2}Mn_{0.6}Ti_{0.2}O_{1.9}F_{0.1}$, were closely examined.

Figure 1a presents the laboratory powder X-ray diffraction (PXRD) pattern obtained on pristine F-DRX powder. All reflections can be indexed to a cubic Fm-3m rock-salt structure. Figure 1b shows the scanning electron microscopy (SEM) images of the pristine F-DRX, revealing uniform, nanosized particles. Particle size analysis (Figure S1) further indicates 94.6% of F-DRX is less than 1 μm with a D10, D50, D90 of 0.172, 0.274, 0.708 μm, respectively.

The overall composition of the nano-sized F-DRX sample was determined by inductively coupled plasma optical emission spectroscopy (ICP-OES) and fluorine ion-selective electrode (F-ISE) measurements. The concentration values of cations through ICP-OES were combined with F concentration (in ppms); yielding a normalized cation ratio of 1.175:0.632:0.193 (Li+Mn+Ti=2) and a cation:fluorine-anion ratio of (Li+Mn+Ti):F = 2.000:0.100. Noticeably, the final F-content was only half of the starting precursor amount of 20 mol%, indicating about 10 mol% of lithium and fluorine content was lost due to LiF volatility during synthesis. At the same time, about 10 mol % of Li loss can be attributed to both LiF and Li_2CO_3 components. It is important to note, however, that compositions derived from ICP/F-ISE analysis may deviate from the actual F-DRX structural composition because impurity phases containing light elements (e.g., Li_2CO_3 and LiF) are not readily detected by laboratory XRD.[19, 31, 32]

To confirm F incorporation into the F-DRX lattice and more accurately determine the composition of the F-DRX phase, ^{7}Li and ^{19}F solid-state nuclear magnetic resonance (ssNMR) measurements were conducted. The ^{7}Li ssNMR spectrum is shown in Figure 1c. A sharp resonance at ~0 ppm corresponds to Li in diamagnetic impurity phases, such as LiF, Li_2CO_3, and Li_2O. In

contrast, the broad and overlapping signals spanning the −200 to 500 ppm frequency range arises from paramagnetic ^{7}Li environments within the DRX structure. A fit of the spectrum (Figure S2) indicates that approximately 86% of the Li in the sample is in a paramagnetic environment in the F-DRX structure, with the remaining 14% present in diamagnetic impurities.

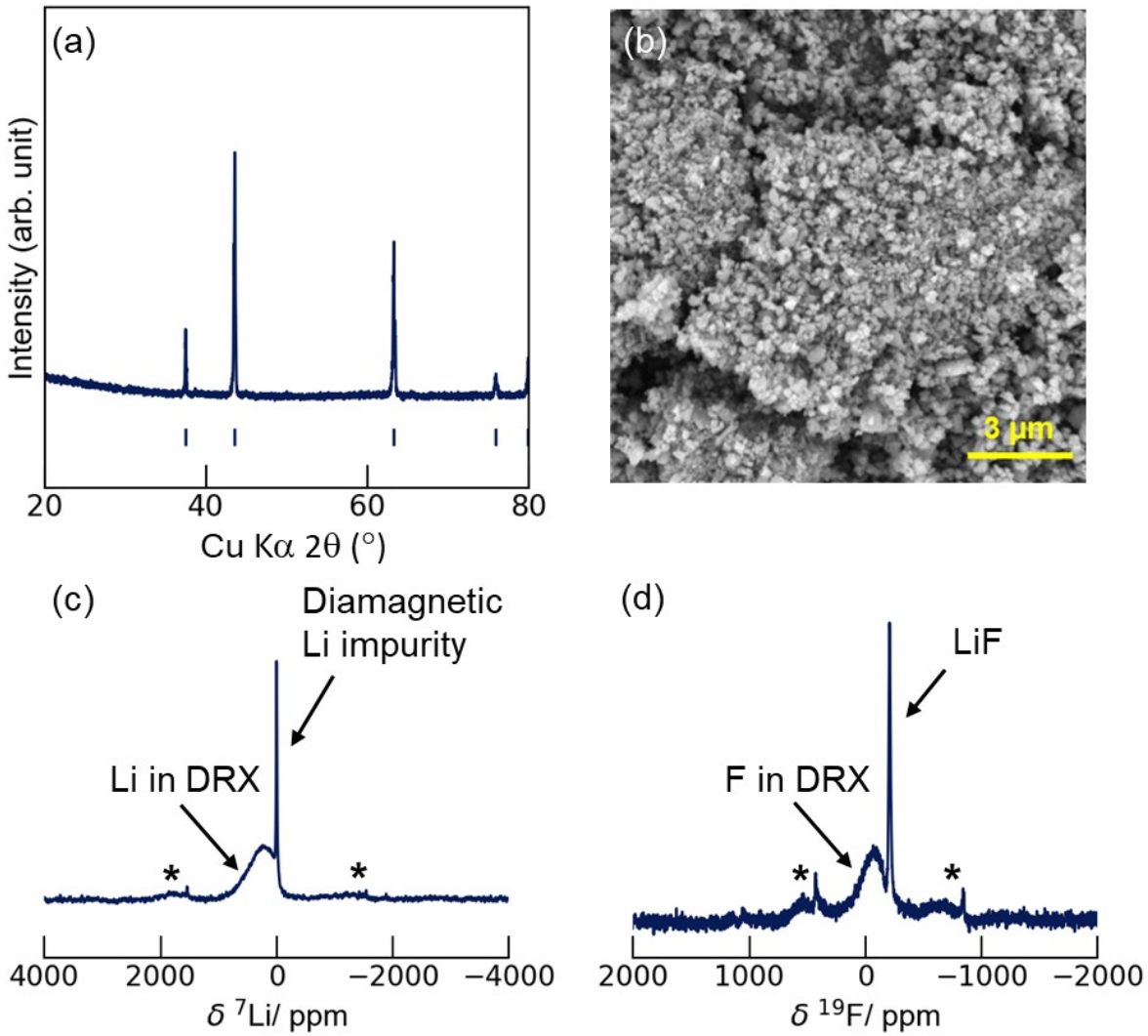

Figure 1. Characterization of the as-synthesized F-DRX material. (a) XRD pattern, (b) SEM micrograph, (c) ^{7}Li and (d) ^{19}F solid-state NMR spectra. NMR spectra were obtained at a 100 MHz (2.35 T) field and at a magic angle spinning (MAS) speed of 60 kHz. The ^{7}Li spectrum was obtained with a 20 s recycle delay, sufficient to ensure full relaxation of all ^{7}Li nuclei in the sample, and is quantitative. The ^{19}F NMR spectrum was obtained with a 20 ms recycle delay to maximize the

paramagnetic signal from F in the F-DRX structure, and is not quantitative. Spinning sidebands are marked with asterisks.

The ^{19}F ssNMR spectrum shown in Figure 1d was obtained using a short recycle delay to maximize the signal intensity from the F-DRX phase and is not quantitative. The sharp signal at −204 ppm is assigned to diamagnetic LiF. The broad resonance spanning the 0 to −500 ppm frequency range arises from paramagnetic ^{19}F environments within the F-DRX structure.[16] A fit of the semi-quantitative ^{19}F spectrum collected with a longer recycle delay of 20 s (Figure S3) yields a lower bound of 55% for the fraction of F residing in the F-DRX phase. As discussed in our recent work,[20] this value underestimates the true fraction because F atoms directly bonded to Mn in the F-DRX phase cannot be observed under the experimental conditions employed here. Based on the distribution of F environments predicted by *ab initio* cluster expansion Monte Carlo simulations for F-DRX ($Li_{1.2}Mn_{0.6}Ti_{0.2}O_{1.8}F_{0.2}$) calcined at 900 °C, approximately 40% of the F atoms are not bonded to Mn and are therefore NMR observable.[19] Applying this correction yields an estimated 76% fraction of F in the F-DRX phase. Combining the corrected NMR results with ICP/F-ISE measurements, the refined chemical formula of pristine F-DRX is estimated to be $Li_{1.1}Mn_{0.69}Ti_{0.21}O_{1.92}F_{0.08}$ (Table S1).

3.2 Voltage- and Electrolyte-Dependent Electrochemical Degradation of F-DRX Cathode

The combined effects of electrolyte chemistry and discharge cutoff voltage on the cycling behavior of the F-DRX are elucidated by conducting a long-term cycling of Li||F-DRX coin cells using the conventional electrolyte and the LHCE in the voltage range of (1.5 – 4.8 V) or (2.0 – 4.8 V). It is worth noting that to eliminate interference from the F-containing polyvinylidene fluoride (PVDF) binder in the sXAS and NMR analyses, a F-free binder, poly(3,4-ethylenedioxythiophene) (PEDOT) is employed in the F-DRX cathode preparation. Since PEDOT generally results in weaker cathode particle adhesion to the aluminum (Al) current collector relative to PVDF, it generally leads to an inferior electrochemical performance compared with the electrode with PVDF. However, this tradeoff is acceptable for the present study as the primary objective is to

isolate and elucidate intrinsic degradation mechanisms in F-DRX cathodes as a function of electrolyte chemistry and discharge voltage.

As shown in Figure 2, the electrochemical performance of Li||F-DRX cells is strongly dependent on the electrolyte formulation. Cells cycled with the LHCE deliver substantially higher initial discharge capacities (260.1 mAh g^{-1} at 2.0 V discharge cutoff, 324.3 mAh g^{-1} at 1.5 V discharge) than those using the conventional electrolyte (213.5 mAh g^{-1} at 2.0 V discharge, 248.4 mAh g^{-1} at 1.5 V discharge). This enhanced initial capacity of F-DRX cathode cycled in LHCE is attributed to reduced parasitic electrolyte decomposition, lower interfacial polarization, enabled by the stable interphase formed in the LHCE, as will be discussed in later sections. More importantly, LHCE-based cells exhibit markedly improved cycling stability, as evidenced by reduced capacity fading and more stable Coulombic efficiencies (Figure S4). These performance advantages are further corroborated by the evolution of direct-current internal resistance (DCIR), which provides insight into the underlying degradation processes. Cells employing the conventional electrolyte show the most pronounced resistance growth (35.6 Ω at the 120^{th} cycle, 2.0 V discharge cutoff), whereas LHCE effectively mitigates the DCIR increase with a value of 4.5 Ω at the 120^{th} cycle, 2.0 V discharge cutoff) consistent with its superior capacity retention (Figure S5).

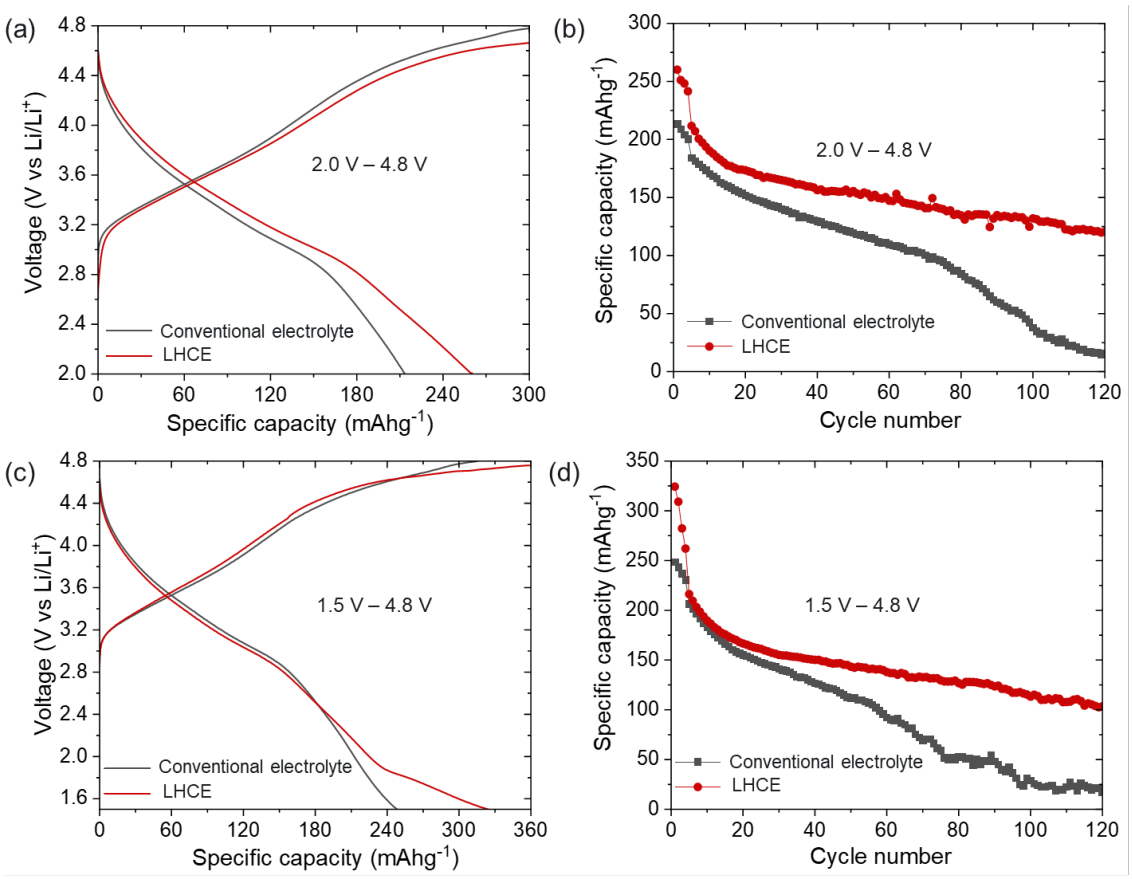

Figure 2. Electrochemical performances of Li||F-DRX coin cells at 30 ºC in the voltage range of (a,b) 2.0– 4.8 V and (c,d) 1.5– 4.8 V. (a,c) 1st cycle charge-discharge voltage profiles and (c,d) long-term cycling stability at 20 mA g^{-1} after four formation cycles at 10 mA g^{-1}.

Lowering the discharge cutoff voltage from 2.0 V to 1.5 V leads to a measurable reduction in capacity retention for both electrolyte systems, particularly at extended cycle numbers. However, the magnitude of this degradation remains relatively modest compared to the dominant influence of electrolyte chemistry. This implies that while the deep discharge to 1.5 V slightly accelerates performance decay relative to cycling at 2.0 V, its effect is secondary to electrolyte-driven instability, with conventional electrolyte-based cells exhibiting both the earlier onset and the more severe capacity loss under all tested conditions. The voltage decay behavior in both voltage windows is presented in Figure S6. The results reveal less voltage decay in the LHCE than in the conventional electrolyte. This is attributed to suppressed interfacial degradation, reduced

impedance growth, and better preservation of the F-DRX structure, which collectively minimizes polarization during long-term cycling. Furthermore, the dQ/dV profiles of the cells with either electrolyte, cycled at both discharge voltages are similar during the first cycle (Figure S7). However, while there is no significant change in the intensity of the peaks in the dQ/dV profiles, there is a more shift in the positions of the redox peaks at higher cycle numbers in the conventional electrolyte than in the LHCE. This observation is consistent with our previous work, which suggested enhanced redox reversibility in the LHCE.[30]

Collectively, these results demonstrate that the long-term electrochemical stability of F-DRX cathode is governed primarily by electrolyte chemistry, while sensitivity to low-voltage operation plays a comparatively minor role within the investigated voltage range.

3.3 Voltage-Induced Interfacial and Bulk Structural Evolution Probed by sXAS

The two variables investigated in this study are electrolyte chemistry and discharge cutoff voltage. Surface side reactions and irreversible redox activity are expected and are known to be closely related to the capacity retention presented in Figure 2. Therefore, sXAS is employed to understand the degree of irreversibility for each variable according to the cycle progress. sXAS uses two modes, total electron yield (TEY) and total fluorescence yield (TFY), which can detect depths of up to 10 nm and 200 nm from the surface, respectively. In particular, it is easy to detect the surface irreversible components such as Li_2CO_3 and LiF including C, O, and F in the energy range of 100 to 2000 eV, and it is specialized in analyzing the oxidation state by detecting empty d-orbitals using the 3d TM L-edge. Also, O and F hybridized to the TM generate peaks in a lower energy region compared to other covalent chemicals, and the hybridization state and redox activity can be estimated based on the changes of these peaks.

Figure 3 is an sXAS analysis targeting the F-DRX cathodes at pristine, 1st, 2nd, 30th, and 60th cycles. This shows the state of the material itself (Pristine), the CEI formation in the first cycle (1st), the state after some hysteresis during the 1st cycle is removed (2nd), and the CEI and redox center activity at the inflection points (30th, 60th) where the contrast of cycle retention presented in Figure 2 occurs.

In the O-K sXAS of Figure 3a and 3b, the TM-O peak highlighted in the green area exhibits broadening and a shift toward lower energy during the charging process, which indicates a decrease in the TM oxidation state. Therefore, if the charge-discharge process remains reversible, repeated peak shifts from low energy to high energy should be observed. Across all studied electrolyte and cutoff conditions, clear shifts of the TM-O peak between charge/discharge states are observed up to the second cycle, where high electrochemical capacity is maintained. By the 30th cycle, however, the specific capacity decreases, and the corresponding TM-O peak movement is also reduced. Nevertheless, because there is no significant difference in the capacity retention for each condition up to the 30th cycle, no pronounced differences appear in the O-K sXAS spectra.

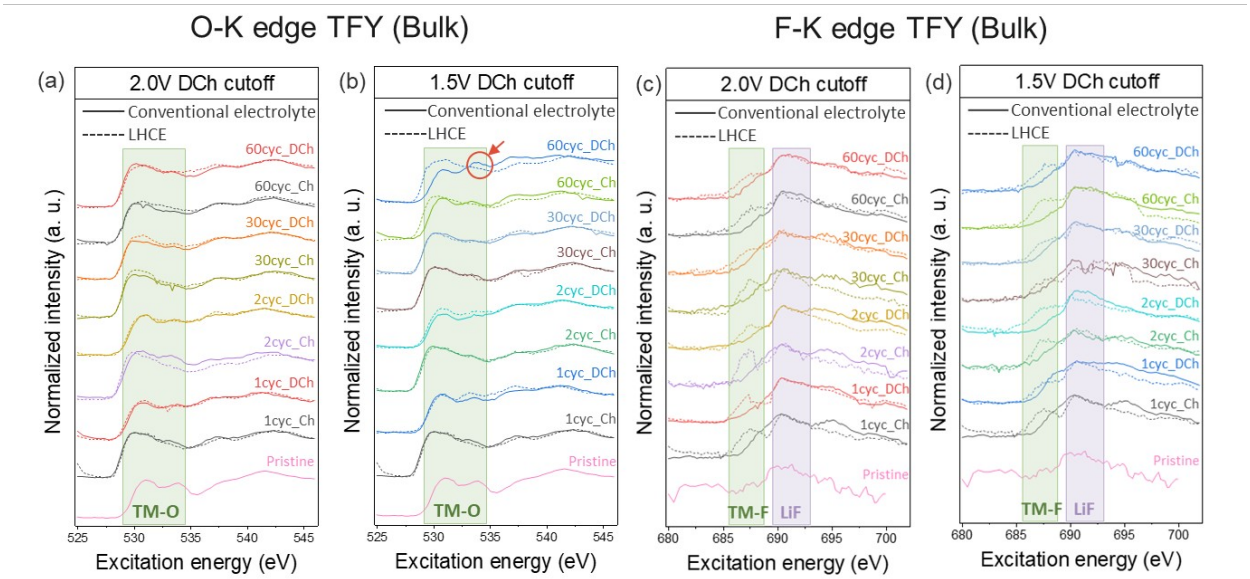

Figure 3. sXAS results of cycled F-DRX cathodes at two discharge voltage cutoffs in conventional electrolyte (solid lines) and LHCE (dotted lines) for (a) O K-edge at 2.0 V discharge cutoff, (b) O K-edge at 1.5 V discharge cutoff, (c) F-K edge at 2.0 V discharge cutoff, and (d) F-K edge at 1.5 V discharge cutoff. The sXAS spectra were collected by TFY mode with TFY probe bulk parts of materials (< 200 nm from the material surface).

At the 60th cycle, the TM-O peak shift becomes a negligible level for all conditions except the 1.5 V discharge cutoff in the conventional electrolyte. Interestingly, this harshest condition, which shows the lowest capacity retention, also exhibits a unique O-K spectral shape. In particular,

the 60cyc_1.5V-DCh spectrum shows a pronounced peak near 534 eV (highlighted by the red arrow), which is not observed in other discharged spectra. This feature strongly suggests the formation of carbonate species, with a very high probability of Li_2CO_3. Figure S8 in the Supporting Information further confirms this interpretation, as the C-K sXAS spectrum shows a strong Li_2CO_3 peak exclusively under this condition. These observations indicate the substantial formation of a surface carbonate layer under this 1.5 V cutoff and conventional electrolyte condition and suggest that the formation of carbonate species may be a key contributor to the rapid capacity decay with cycling. It is also noteworthy that such carbonate surface formation is not happening in the LHCE regardless of discharge cutoff conditions during cycling. Specifically, a closer examination of the O K-edge TFY spectra reveals a subtle but critical energy shift between the initial and prolonged cycles. After the 1st cycle, a minor feature appears at approximately 533 eV (Figure 3b). While this energy region can overlap with the π^* transitions of organic carbonates or the e_g bands of transition metal oxides,[33] this initial feature did not exhibit a clear correlation with long-term capacity fade. In contrast, the prominent peak that dominates after 60 cycles is centered at about 534 eV, showing a roughly 1 eV upward shift compared to the 1st-cycle feature. According to previous literature, this peak near 534 eV is uniquely indexed to the π^* orbital excitation of metal carbonates, specifically Li_2CO_3 under the given discharged state (1.5 V).[34] This distinction confirms that the critical path of material degradation is associated with the substantial accumulation of Li_2CO_3 during extended cycling, rather than its initial formation in the early cycles.

A similar trend of interfacial degradation was further substantiated by the surface-sensitive TEY mode (Figure S9). Under the most electrochemically unfavorable condition, namely, 60 cycles in the conventional electrolyte with a 1.5 V cutoff, the TEY spectrum exhibits a highly pronounced feature that closely resembles the signature of heavily decomposed electrolyte layers typically observed in deeply discharged SEI films.[33, 35] Although a precise decoupling of overlapping organic and inorganic species is inherently complex, the dominance of this decomposition signal clearly underscores the severe interfacial breakdown and parasitic electrolyte consumption occurring under conventional electrolyte environments.

As noted earlier, this study employs a binder that does not contain F in order to analyze the behavior of F within the cathode material. This choice enables the use of F-selective sXAS and the

results of the F-K edge are shown in Figure 3c and 3d. Due to the low F concentration in F-DRX, the overall low signal-to-noise (S/N) ratio of the spectra is not good, but the overall trend is identifiable. The pristine state shows a specifically bad S/N ratio, and this is likely due to impurity species present on the pristine surface that interfere with detection. The carbonate species observed in the pristine O-K and C-K spectra as shown in Figures 3a, 3b, S8, and S9 may also contribute to this interference.

Similar to the TM-O pre-edge appearing at lower energy than the main O-K edge (beyond 535 eV), the TM-F feature (highlighted by the green rectangle in Figure 3c, 3d, and Figure S10) is observed at lower energy relative to the F-K edge. Interestingly, the F-K spectra from the LHCE and conventional electrolyte show a strong contrast in terms of the pre-edge intensity. In LHCE, the TM-F pre-edge remains as a distinct and prominent peak throughout cycling. In contrast, in the conventional electrolyte, this peak appears significantly weaker and is mostly observed as a shoulder superimposed on the LiF intensity. Moreover, the TM-F peak in the conventional electrolyte gradually diminishes with continued cycling. The contrast between TM-F and Li-F is more distinguished on their surface, as shown in Figure S10. There is renowned formation of LiF-like domain at the surface region of F-DRX,[36] and the relative peak intensity of LiF against TM-F is expected to be higher than the bulk, which is clearly demonstrated in Figure S10. Consequently, the LHCE system helps the F introduced during the synthesis process remain in a state coordinated to the TM even during operation. Generally, it is known that the reason F-doping increases cathode performance lies in the intrinsic property changes due to F coordination. Considering this, the reason LHCE shows superior cycle performance compared to the conventional electrolyte is very likely because this F coordination state was sustained.

In Figure 4, the cycled F-DRX electrodes compared with the pristine correspond to fully charged states after 60 cycles under each electrolyte and cutoff condition. As referred above, the Mn-L_3 edge is a direct measure of the oxidation state for Mn based on the unique spectral shapes of each Mn oxidation state. In Figure 4b, map of resonant inelastic X-ray scattering-inverse partial fluorescence yield (mRIXS-iPFY) was used instead of TFY due to the spectral distortion of Mn-L TFY spectra by the O-K fluorescence.[30]

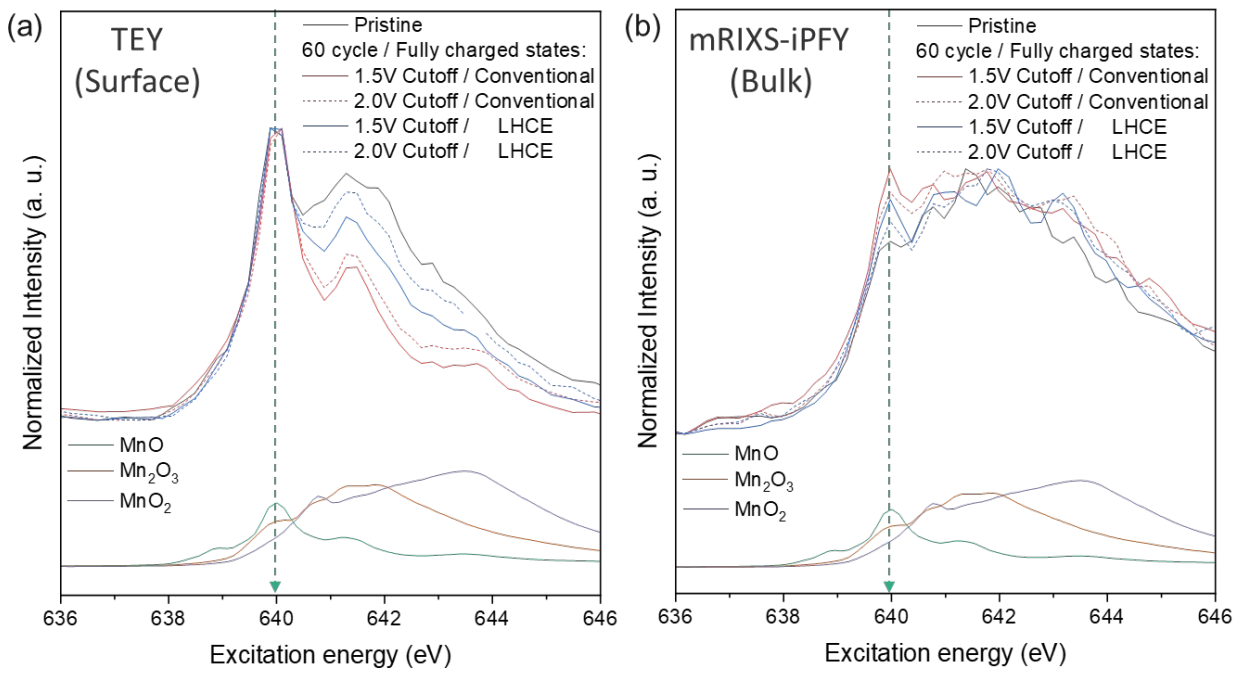

Figure 4. sXAS results of cycled cathodes at 1.5 V discharge voltage cutoffs (solid lines), at 2.0 V discharge voltage cutoff (dotted lines) in conventional electrolyte and LHCE for Mn L_3-edge. The sXAS spectra were collected by (a) TEY mode and (b) mRIXS-iPFY mode.

The TEY and mRIXS-iPFY spectra show the degree of Mn redox inactivation depending on the cell operation environment. Across these electrodes, the intensity differences in the Mn^{2+} peak associated with MnO are clearly observed (highlighted by the green dashed line). There is a renowned reconstruction of the cathode surface, so called densification, including reduction of the transition metals at the surface and the subsurface of cathode materials. Considering the electrodes are fully charged, the relative intensity of Mn^{2+} components could be directly correlated to the redox inactive Mn. The trend of Mn^{2+} relative peak intensity appears to correlate well with the electrochemical cycle retention. The ordering of oxidation states, from the highest in the 2.0 V discharge cutoff and LHCE conditions (which shows the best retention) to the lowest in the 1.5 V discharge cutoff and conventional electrolyte (which shows the poorest retention), corresponds directly to the observed cycling performance.

3.4 Coupled Surface and Bulk Structural Degradation on Deep Discharge

Nanoscale structural changes induced by deep discharge were examined using STEM and solid-state NMR. Together, these techniques reveal surface and bulk structural degradation, as previously observed for the case of Li-rich layered cathode,[37] and DRX cathode.[38]

High-angle annular dark-field STEM (HAADF-STEM) imaging of the F-DRX particles collected after 120 cycles and corresponding energy dispersive X-ray spectroscopy (EDS) data reveal significant structural damage in the conventional electrolyte (Figure 5a). This manifests as formation of cracks (yellow arrows in Figure S9) and voids as evidenced by the dark contrast in the HAADF images of Figures 5a and S9, indicative of pronounced mechanical and chemical degradation. In contrast, the F-DRX particles cycled in LHCE exhibit markedly suppressed crack formation and voids development as evidenced by the HAADF image of Figure 5b. While both samples exhibit a comparable CEI layer revealed by the EDS maps of the characteristic elements P for conventional electrolyte and S in LHCE (Figure S12), the cathodes cycled in the conventional electrolyte exhibit more structural damage, typifying a high density of nanovoid formation as a consequence of gradual oxygen and transition metal loss and vacancies injection.[37, 38] This observation demonstrates that LHCE effectively stabilizes the cathode surface and preserves the mechanical integrity of F-DRX particles during prolonged cycling. This is consistent with prior reports where LHCEs have been demonstrated to preserve the mechanical integrity of high voltage cathodes.[29, 30]

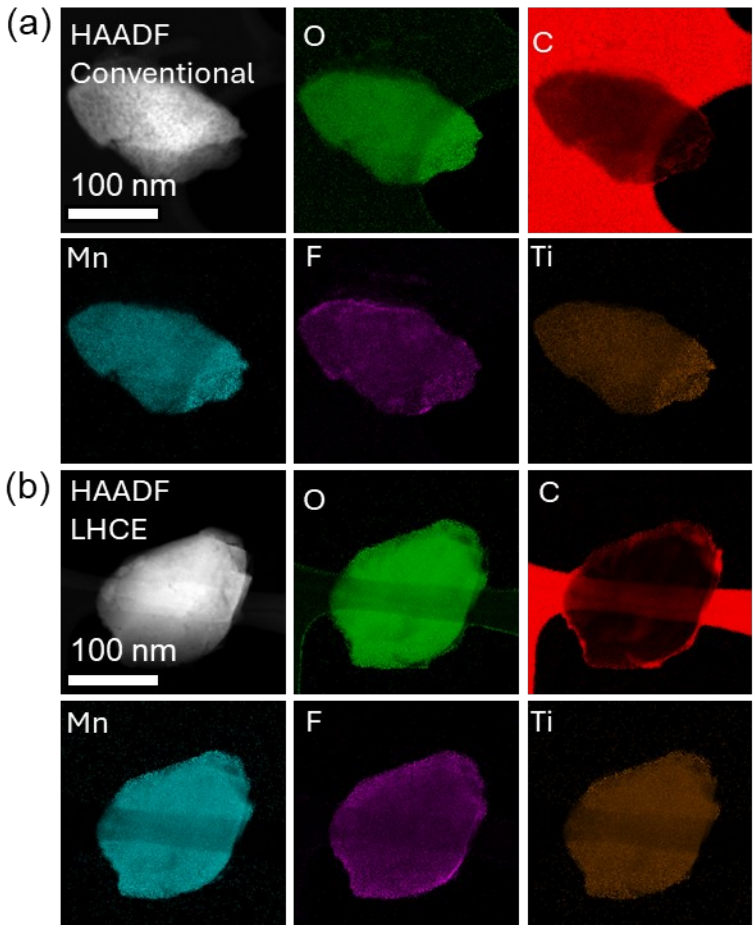

Figure 5. STEM and EDS results of cycled cathodes collected after 120 cycles in the voltage range 1.5 V – 4.8 V, in (a) conventional electrolyte and (b) LHCE. The dark contrast spots in HAADF of (a) correspond to nanovoid, which is absent in the HAADF image of (b) when LHCE is used.

Complementary insights into the evolution of the local structure are obtained by comparing the ^{7}Li NMR spectra for the pristine powder and cycled F-DRX cathodes extracted from cells discharged to 1.5 V after 120 cycles (Figure 6). The spectra are quantitative and were normalized to both the number of scans and the electrode mass, enabling a direct comparison of the signal intensities.

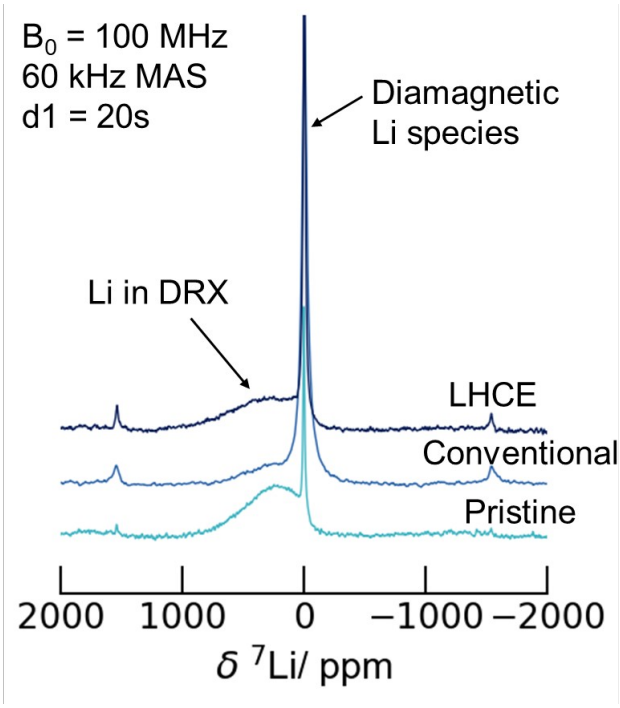

Figure 6. ^{7}Li solid-state NMR spectra collected on pristine F-DRX (bottom), and on two ex situ F-DRX samples discharged to 1.5 V after 120 cycles: when using a conventional electrolyte (middle), and when using a LHCE (top). Spectra were obtained with a 20 s recycle delay, sufficiently long to ensure full relaxation of all ^{7}Li nuclei in the sample, and are quantitative.

Fits of the spectra are shown in Figure S2 and provide additional information about changes in the chemical shifts and broadening of the NMR resonances upon cycling. As mentioned earlier, the pristine ^{7}Li NMR spectrum can be fit using a minimum of two resonances centered at 130 and 360 ppm, with linewidths of 9.1 and 18.4 kHz, attributed to F in the F-DRX structure, and a sharp resonance at 0 ppm assigned to diamagnetic Li-containing phases. The *ex situ* ^{7}Li spectrum obtained after cycling in the conventional electrolyte can be fit using a single broad ^{7}Li resonance centered at 120 ppm (28.7 kHz linewidth), with a significantly reduced intensity compared to the two paramagnetic resonances in the pristine spectrum, indicating substantial Li inventory loss or impedance build-up reducing Li reinsertion. Meanwhile, the sharp resonance at ~0 ppm increases in intensity and broadens (from 0.65 kHz in the pristine to 2.1 kHz in the *ex situ* spectrum), presumably due to the presence of residual electrolyte degradation products at the surface of the (washed) electrode sample. The *ex situ* ^{7}Li spectrum obtained after cycling in the LHCE can be fit

with a single broad ^{7}Li resonance centered at 310 ppm (25.1 kHz linewidth); while the intensity of the paramagnetic resonance is reduced compared to that of the pristine spectrum, signal loss is much less severe than when the F-DRX cathode is cycled in the conventional electrolyte. The broadening on the sharp resonance at ~0 ppm is also not as obvious (0.89 kHz linewidth), suggesting less extensive electrolyte or DRX structural degradation. These findings are consistent with STEM analysis, which confirms that the mechanical integrity of electrodes cycled in LHCE is largely preserved, whereas significant structural degradation occurs in electrodes cycled in the conventional electrolyte.

Collectively, these results indicate a degradation mechanism in which deep discharge induces a surface disorder accompanied by a significant bulk local-environment changes, while the electrolyte chemistry plays a decisive role in regulating the propagation of these effects, with the LHCE markedly suppressing these structural changes. This behavior is consistent with recent studies on electrolyte-regulated degradation and interfacial modification in Li-rich layered cathodes [39, 40], which demonstrated that electrolyte-derived interphases can strongly influence surface reconstruction, transition-metal migration, and the propagation of structural degradation into the bulk. The formation of a more stable and protective cathode-electrolyte interphase can suppress parasitic interfacial reactions and mitigate surface-to-bulk structural evolution, thereby improving the structural stability of the cathode during cycling.

3.5 Mechanistic Framework and Design Implications

Integrating electrochemical performance results, resistance evolution, and multi-modal structural characterization data establishes a coherent mechanistic framework for F-DRX degradation that is strongly governed by electrolyte chemistry. These degradation mechanisms of F-DRX cycled in both electrolyte chemistries are summarized in Figure 7.

In LHCE-based systems, there is a stabilization of both surface and bulk structures, thereby suppressing resistance growth and mitigating structural degradation of F-DRX. In contrast, the conventional electrolyte promotes increasingly irreversible redox behavior, generates a higher fraction of Mn^{2+} during charge, forming more densified domains on the cathode surface that are

electrochemically inactive towards Li^+ intercalation. Furthermore, the use of a conventional electrolyte induces a substantial Li inventory loss. These phenomena manifest as surface and bulk structural degradation and progressive impedance growth, ultimately accelerating capacity fade. Although deep discharge exacerbates the degradation mechanisms, its impact is secondary to that of electrolyte chemistry, as reflected in the electrochemical performance of F-DRX-based cells.

These findings identify two key design principles for stabilizing F-DRX cathodes: (i) electrolyte engineering to minimize interfacial reactivity, suppress local structural disorder, and reduce Li inventory loss, thereby preserving the mechanical and electrochemical integrity of the cathode; and (ii) voltage-window optimization to avoid deep-discharge regimes that promote both surface and bulk structural degradation. More broadly, the results underscore that durable DRX operation requires the co-design of cathode composition, electrolyte formulation, and cycling protocol, with LHCE-type electrolytes offering a promising pathway toward stable, high-energy DRX-based LIBs.

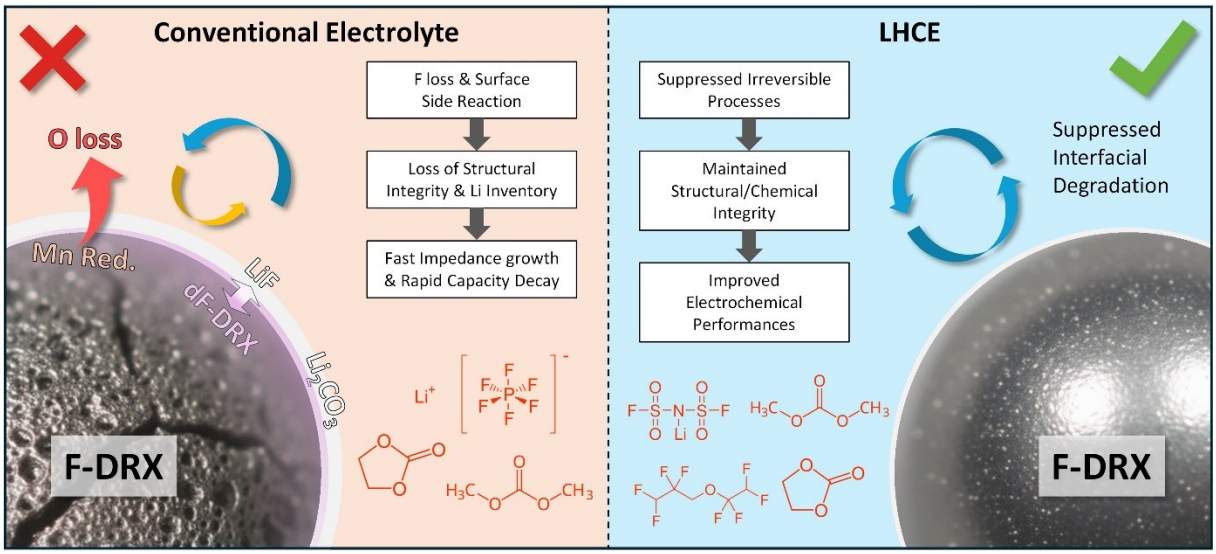

Figure 7. Schematic illustration of degradation mechanisms of F-DRF cycled in conventional electrolyte and LHCE.

4. Conclusion

This study establishes a mechanistic framework for voltage- and electrolyte-dependent degradation in F-doped DRX cathodes by directly correlating redox evolution, TM chemistry, and nanoscale structural integrity with macroscopic electrochemical performance. The results show that, despite F incorporation into the DRX cathode, the use of conventional $LiPF_6$-carbonate electrolyte promotes increasingly irreversible redox behavior and accelerates cation rearrangement causing a significant loss of Li ion inventory. This gives rise to coupled surface and bulk structural distortion and rapid impedance growth that ultimately leads to a fast capacity decay in Li||F-DRX cells. In sharp contrast, the LHCE effectively preserves redox reversibility and suppresses both interfacial and bulk structural degradation, enabling markedly improved electrochemical stability. Deep discharge to 1.5 V further amplifies irreversible redox activity particularly in the conventional electrolyte relative to 2.0 V cutoff, thereby exacerbating resistance growth and capacity fade. Nevertheless, the magnitude of this voltage-induced degradation remains secondary to the dominant influence of electrolyte chemistry. Overall, these findings demonstrate that a stable operation of F-DRX cathodes requires simultaneous optimization of electrolyte chemistry and cycling protocols and position LHCE-type electrolytes as a promising strategy for enabling stable, high-energy Li batteries based on DRX cathodes.

ASSOCIATED CONTENT

Supporting Information.

The following files are available free of charge.

Particle size analysis; Fits of the ^{7}Li and ^{19}F solid-state NMR spectra; cycling performance data; sXAS results, quantitative linear combination fitting of Mn L_3-edge spectra; STEM EDS of cycled F-DRX (Word)

Conflict of interest statement

The authors declare no conflicts of interest.

AUTHOR INFORMATION

Corresponding Authors

Raphaële J. Clément – Materials Department and Materials Research Laboratory, University of California Santa Barbara, CA 93106, USA; Email: rclement@ucsb.edu

Wanli Yang – Advanced Light Source, Lawrence Berkeley National Laboratory, Berkeley, CA 94720, USA, Email: wlyang@lbl.gov

Chongmin Wang – Environmental Molecular Sciences Laboratory, Pacific Northwest National Laboratory Richland, WA 99354, USA; E-mail: chongmin.wang@pnnl.gov

Wu Xu – Energy and Environment Directorate Pacific Northwest National Laboratory Richland, WA 99354, USA; Email: wu.xu@pnnl.gov

Author Contributions

Ridwan A. Ahmed and Gi-Hyeok Lee: Conceptualization, Methodology, Formal analysis, Data curation, Writing – Original draft. **Eitan Hershkovitz, Tianyu Li, Yanbao Fu, Isiksu Buyuker, and Mateusz Zuba:** Methodology, Data curation, Writing – Review and editing. **Ozgenur Kahvecioglu and Vincent S. Battaglia:** Funding acquisition, Writing – Review and editing. **Raphaële J. Clément, Wanli Yang, Chongmin Wang, and Wu Xu:** Conceptualization, Funding acquisition, Project administration, Supervision, Writing – Review and editing.

ACKNOWLEDGMENTS

This work was funded by the Transportation Technologies Office of the U.S. Department of Energy (DOE) through the DRX+ Consortium under the contract no. DE-AC05-76RL01830 for Pacific Northwest National Laboratory (PNNL), DEAC02-05CH11231 for Lawrence Berkeley National Laboratory (LBNL), and DE-AC02-06CH11357 for Argonne National Laboratory (ANL). Part of the microscopic and spectroscopic characterizations were performed in the William R. Wiley Environmental Molecular Sciences Laboratory (EMSL), a national scientific user facility sponsored by DOE's Office of Biological and Environmental Research and located at PNNL. Part of the electron microscopy work was carried out by using instruments that are funded in part by a grant from the Washington State Department of Commerce's Clean Energy Fund. PNNL is operated by Battelle for the DOE under Contract DE-AC05-76RL01830. This work made use of the shared MRL Spectroscopy facility of the UC Santa Barbara MRSEC (DMR 2308708), a member of the Materials Research Facilities Network. The LMTF cathode material synthesis reported in this paper was performed at the Materials Engineering Research Facility (EMRF), ANL. The MERF was supported by the DOE, Office of Energy Efficiency and Renewable Energy, and the Vehicle Technologies Office. Soft X-ray experiments were performed at BL 8.0.1 of the Advanced Light Source (ALS), a DOE Office of Science User Facility, under contract no. DE-AC02-05CH11231. G.-H. Lee acknowledges the support from the U.S. DOE, Office of Science, Office of Basic Energy Sciences program under Award Number DE-SC0024404. The salt LiFSI was provided by Dr. Kazuhiko Murata of Nippon Shokubai Co., Ltd.

REFERENCES

(1) Gourley, S. W. D.; Or, T.; Chen, Z. Breaking Free from Cobalt Reliance in Lithium-Ion Batteries. *iScience* **2020**, *23* (9), 101505.
(2) Keshari, N.; Dewangan, T.; Basu, K.; Gandharv, T.; Kumar, N.; Panda, P.; Nanaji, K. Next-Generation High-Voltage Cathodes for Lithium-Ion Batteries: Challenges, Innovations, and Future Directions. *Advanced Sustainable Systems* **2025**, *9* (10), e00543.
(3) Clément, R. J.; Lun, Z.; Ceder, G. Cation-disordered rocksalt transition metal oxides and oxyfluorides for high energy lithium-ion cathodes. *Energy & Environmental Science* **2020**, *13* (2), 345-373.
(4) Ahn, J.; Ha, Y.; Satish, R.; Giovine, R.; Li, L.; Liu, J.; Wang, C.; Clement, R. J.; Kostecki, R.; Yang, W.; et al. Exceptional Cycling Performance Enabled by Local Structural Rearrangements in Disordered Rocksalt Cathodes. *Advanced Energy Materials* **2022**, *12* (27), 2200426.
(5) Chen, D.; Ahn, J.; Chen, G. An Overview of Cation-Disordered Lithium-Excess Rocksalt Cathodes. *ACS Energy Letters* **2021**, 1358-1376.
(6) Li, H.; Fong, R.; Woo, M.; Ahmed, H.; Seo, D.-H.; Malik, R.; Lee, J. Toward high-energy Mn-based disordered-rocksalt Li-ion cathodes. *Joule* **2022**, *6* (1), 53-91.
(7) Cai, Z.; Ouyang, B.; Hau, H.-M.; Chen, T.; Giovine, R.; Koirala, K. P.; Li, L.; Ji, H.; Ha, Y.; Sun, Y.; et al. In situ formed partially disordered phases as earth-abundant Mn-rich cathode materials. *Nature Energy* **2023**. *9*, 27-36.
(8) Zhang, H.; Gao, X.; Cai, Q.; Zhang, X.; Tian, Y.; Jia, M.; Xie, W.; Du, Y.; Yan, X. Recent progress and perspectives on cation disordered rock-salt material for advanced Li-ion batteries. *Journal of Materials Chemistry A* **2023**, *11* (16), 8426-8452.
(9) Thackeray, M. M.; Croy, J. R.; Lee, E.; Gutierrez, A.; He, M.; Park, J. S.; Yonemoto, B. T.; Long, B. R.; Blauwkamp, J. D.; Johnson, C. S.; et al. The quest for manganese-rich electrodes for lithium batteries: strategic design and electrochemical behavior. *Sustainable Energy & Fuels* **2018**, *2* (7), 1375-1397.
(10) Chung, H.; Lebens-Higgins, Z.; Sayahpour, B.; Mejia, C.; Grenier, A.; Kamm, G. E.; Li, Y.; Huang, R.; Piper, L. F. J.; Chapman, K. W.; et al. Experimental considerations to study Li-excess disordered rock salt cathode materials. *Journal of Materials Chemistry A* **2021**, *9* (3), 1720-1732.
(11) Luo, M.; Zheng, S.; Wu, J.; Zhou, K.; Zuo, W.; Feng, M.; He, H.; Liu, R.; Zhu, J.; Zhao, G.; et al. Identifying the anionic redox activity in cation-disordered $Li_{1.25}Nb_{0.25}Fe_{0.50}O_2$/C oxide cathodes for Li-ion batteries. *Journal of Materials Chemistry A* **2020**, *8* (10), 5115-5127.
(12) Chen, D.; Kan, W. H.; Chen, G. Understanding Performance Degradation in Cation-Disordered Rock-Salt Oxide Cathodes. *Advanced Energy Materials* **2019**, *9* (31), 1901255.

(13) Li, Q.; Wang, Y.; Wang, X.; Sun, X.; Zhang, J. N.; Yu, X.; Li, H. Investigations on the Fundamental Process of Cathode Electrolyte Interphase Formation and Evolution of High-Voltage Cathodes. *ACS Appl Mater Interfaces* **2020**, *12* (2), 2319-2326.
(14) Zhou, K.; Zhang, C.; Li, Y.; Liu, X.; Liu, J.; Lun, Z.; Yang, Y. A Critical Evaluation of Interfacial Stability in Li-excess Cation-disordered Rock-salt Oxide Cathode. *Chemical Engineering Journal* **2023**, *464*, 142709.
(15) House, R. A.; Jin, L.; Maitra, U.; Tsuruta, K.; Somerville, J. W.; Förstermann, D. P.; Massel, F.; Duda, L.; Roberts, M. R.; Bruce, P. G. Lithium manganese oxyfluoride as a new cathode material exhibiting oxygen redox. *Energy & Environmental Science* **2018**, *11* (4), 926-932.
(16) Clément, R. J.; Kitchaev, D.; Lee, J.; Gerbrand, C. Short-Range Order and Unusual Modes of Nickel Redox in a Fluorine-Substituted Disordered Rocksalt Oxide Lithium-Ion Cathode. *Chemistry of Materials* **2018**, *30* (19), 6945-6956.
(17) Yue, Y.; Li, N.; Ha, Y.; Crafton, M. J.; McCloskey, B. D.; Yang, W.; Tong, W. Tailoring the Redox Reactions for High-Capacity Cycling of Cation-Disordered Rocksalt Cathodes. *Advanced Functional Materials* **2021**, *31* (14), 2008696.
(18) Lee, G. H.; Lim, J.; Shin, J.; Hardwick, L. J.; Yang, W. Towards commercialization of fluorinated cation-disordered rock-salt Li-ion cathodes. *Front Chem* **2023**, *11*, 1098460.
(19) Wu, V. C.; Zhong, P.; Ong, J.; Yoshida, E.; Kwon, A.; Ceder, G.; Clement, R. J. The Limited Incorporation and Role of Fluorine in Mn-rich Disordered Rocksalt Cathodes. *ACS Energy Lett* **2024**, *9* (6), 3027-3035.
(20) Giovine, R.; Yoshida, E.; Wu, V. C.; Ji, Y.; Crafton, M. J.; McCloskey, B. D.; Clement, R. J. An Experimental Approach to Assess Fluorine Incorporation into Disordered Rock Salt Oxide Cathodes. *Chem Mater* **2024**, *36* (8), 3643-3654.
(21) Ahn, J.; Chen, D.; Chen, G. A Fluorination Method for Improving Cation-Disordered Rocksalt Cathode Performance. *Advanced Energy Materials* **2020**, *10* (35), 2001671.
(22) Szymanski, N. J.; Zeng, Y.; Bennett, T.; Patil, S.; Keum, J. K.; Self, E. C.; Bai, J.; Cai, Z.; Giovine, R.; Ouyang, B.; et al. Understanding the Fluorination of Disordered Rocksalt Cathodes through Rational Exploration of Synthesis Pathways. *Chemistry of Materials* **2022**, *34* (15), 7015-7028.
(23) Yue, Y.; Ha, Y.; Giovine, R.; Clément, R.; Yang, W.; Tong, W. High-Voltage Reactivity and Long-Term Stability of Cation-Disordered Rocksalt Cathodes. *Chemistry of Materials* **2022**, *34* (4), 1524-1532.
(24) Liu, Y.; Wu, X.; Feng, H.; Lu, G.; Jiang, Y.; Lou, X.; Li, C.; Shen, M.; Geng, F.; Hu, B. Interfacial deterioration in highly fluorinated cation-disordered rock-salt cathode: Carbonate-based electrolyte vs. ether-based electrolyte. *Energy Storage Materials* **2024**, *73*, 103789.
(25) Lynn, H. L.; Denison, B. M. G.; Jones, K. D.; Leesmith, M. J. A.; Hua, X.; Johnson, L. R.; Tapia Ruiz, N. Unravelling the Degradation Mechanism in Fluorinated Disordered Rock-Salt Cathodes for Lithium-Ion Batteries. *ECS Meeting Abstracts* **2025**, *2025*, 271-271.
(26) Cao, X.; Jia, H.; Xu, W.; Zhang, J.-G. Review—Localized High-Concentration Electrolytes for Lithium Batteries. *Journal of The Electrochemical Society* **2021**, *168* (1), 010522.
(27) Weintz, D.; Werres, M.; Horstmann, B.; Amine, R.; Su, C.-C.; Li, X.; Xu, Y.; Ahmed, R. A.; Xu, W.; Wang, C.; et al. Nanoengineering of non-aqueous liquid electrolyte solutions for future lithium metal batteries. *Nature Nanotechnology* **2026**, *21*, 336-351

(28) Ahmed, R. A.; Song, M.; Tao, L.; Yao, J.; Xu, Y.; Engelhard, M. H.; Weller, J. M.; Guo, Y.; Ver Beek, C.; Kautz, D.; et al. Electrolytes for Fast-Charging Lithium-Ion Batteries with a Disordered Rock Salt Cathode. *ACS Applied Energy Materials* **2026**, *9,* 5069-5077.
(29) Ahmed, R. A.; Mohanakrishnan, R. S.; Wang, J.; Koirala, K. P.; Zhao, Q.; Fu, Y.; Chen, Y.; Rastinejad, J. C.; Li, T.; Zhong, L.; et al. Designing Advanced Electrolytes for High-Voltage High-Capacity Disordered Rocksalt Cathodes. *Small* **2025**, *21* (18), 2501600.
(30) Ahmed, R. A.; Koirala, K. P.; Lee, G. H.; Li, T.; Zhao, Q.; Fu, Y.; Zhong, L.; Daddona, J. D.; Zuba, M.; Siu, C.; et al. Enhanced Electrochemical Performance of Disordered Rocksalt Cathodes in a Localized High-Concentration Electrolyte. *Advanced Energy Materials* **2024**, *14* (27), 2400722.
(31) Avvaru, V. S.; Li, T.; Lee, G.-H.; Byeon, Y.-W.; Koirala, K. P.; Marques, O. J.; Rinkel, B. L. D.; Fu, Y.; Milsted, D.; Jeong, S.; et al. Alternative Solid-State Synthesis Route for Highly Fluorinated Disordered Rock-Salt Cathode Materials for High-Energy Lithium-Ion Batteries. *Advanced Energy Materials* **2025**, *15* (28), 2500492.
(32) Giovine, R.; Yoshida, E.; Wu, V. C.; Ji, Y.; Crafton, M. J.; McCloskey, B. D.; Clment, R. J. An Experimental Approach to Assess Fluorine Incorporation into Disordered Rock Salt Oxide Cathodes. *Chemistry of Materials* **2024**, *36* (8), 3643-3654.
(33) Swallow, J. E. N.; Fraser, M. W.; Kneusels, N.-J. H.; Charlton, J. F.; Sole, C. G.; Phelan, C. M. E.; Björklund, E.; Bencok, P.; Escudero, C.; Pérez-Dieste, V.; et al. Revealing solid electrolyte interphase formation through interface-sensitive Operando X-ray absorption spectroscopy. *Nature Communications* **2022**, *13* (1), 6070.
(34) Frati, F.; Hunault, M.; de Groot, F. M. F. Oxygen K-edge X-ray Absorption Spectra. *Chem Rev* **2020**, *120* (9), 4056-4110.
(35) Panajotović, R.; Ptasinska, S.; Lyamayev, V.; Prince, K. Low-Energy Electron Damage of Dppc Molecules – a Nexafs Study. *RAD Association Journal* **2016**. *1*, 46-50
(36) Chen, D.; Ahn, J.; Self, E.; Nanda, J.; Chen, G. Understanding cation-disordered rocksalt oxyfluoride cathodes. *Journal of Materials Chemistry A* **2021**, *9* (12), 7826-7837.
(37) Yan, P.; Zheng, J.; Tang, Z.-K.; Devaraj, A.; Chen, G.; Amine, K.; Zhang, J.-G.; Liu, L.-M.; Wang, C. Injection of oxygen vacancies in the bulk lattice of layered cathodes. *Nature Nanotechnology* **2019**, *14* (6), 602-608.
(38) Li, L.; Ahn, J.; Yue, Y.; Tong, W.; Chen, G.; Wang, C. Fluorination-Enhanced Surface Stability of Disordered Rocksalt Cathodes. *Advanced Materials* **2022**, *34* (12), 2106256.
(39) Che, H.; Su, Y.; Dong, J.; Lu, Y.; Hao, J.; Wang, Y.; Yang, T.; He, X.; Wu, Y.; Li, N.; et al. A whole greater than the sum of its parts: composite-electrolyte-induced rigid-adaptive interphase for stabilizing a lithium-rich cathode. *Energy Storage Materials* **2026**, *86*, 105020.
(40) Che, H.; Su, Y.; Dong, J.; Lei, W.; Lu, Y.; Hao, J.; Wang, Y.; Yang, T.; He, X.; Wu, Y.; et al. Integrated bulk-interphase synergy strategy for structural integrity and high-rate durability in lithium-rich manganese cathodes. *Journal of Energy Chemistry* **2026**, *119*, 821-834.

ToC Figure

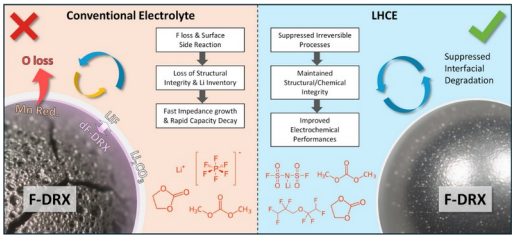
Conventional Electrolyte
O loss
Mn Red.
LiF
dF DRX
Li2CO3
F-DRX
F loss & Surface Side Reaction
Loss of Structural Integrity & Li Inventory
Fast Impedance growth & Rapid Capacity Decay
LHCE
Suppressed Irreversible Processes
Maintained Structural/Chemical Integrity
Improved Electrochemical Performances
Suppressed Interfacial Degradation
F-DRX